Two-step process of cytoskeletal structural damage during long-term storage of packed red blood cells

Elena Kozlova[1,2], Aleksandr Chernysh[1,2], Viktor Moroz[1], Aleksandr Kozlov[2], Viktoria Sergunova[1], Ekaterina Sherstyukova[1,2], Olga Gudkova[1]

[1]*V.A. Negovsky Research Institute of General Reanimatology, Federal Research and Clinical Center of Intensive Care Medicine and Rehabilitology, Moscow, Russian Federation;*
[2]*Sechenov First Moscow State Medical University (Sechenov University), Moscow, Russian Federation*

Background - Storage of packed red blood cells (PRBC) for 42 days causes morphological, structural, and functional changes in the red cells. To assess the quality of stored PRBC, it is important to evaluate the main components of the product. The aim of this study was to evaluate the kinetics of the structural transformations in the cytoskeleton of red cells during long-term storage (up to 42 days).

Materials and methods - Bags of PRBC were stored with CPD/SAGM solution at +4 °C. Cytoskeletal parameters were measured on days 3, 12, 19, 21, 24, 28, 35, and 42 of storage to determine their changes. Atomic force microscopy was used to obtain images and analyse the parameters of the cytoskeletal network. As the storage time increased, a general PRBC test was performed. Membrane fixatives were not used at any stage of the preparation of the specimens for cytoskeletal imaging.

Results - When PRBC were stored for 42 days, the main changes to the cytoskeletal mesh included rupture of filaments, merger of small pores into larger ones, a decrease of the number of pores, thickening of filaments, and an increase of membrane stiffness. A process of irreversible changes to the cytoskeleton started on days 19-21. A kinetic model of changes in the parameters of the cytoskeletal mesh with time of PRBC storage was created.

Discussion - Two stages of impairment in cytoskeletal elements were found: rupture of filaments and clustering of protein components. The typical time of development and specifics of these stages are discussed. The consequences of the altered configuration of the cytoskeleton are also discussed. Destruction of the red cell cytoskeleton can have a negative effect on the efficacy of blood transfusion and increase the risk of post-transfusion complications. Our findings can be used in clinical medicine to evaluate the quality of PRBC for blood transfusion as well as for studies of the molecular organisation of red cells undergoing various types of physical and chemical treatment.

Keywords: *packed red blood cells, long-term storage, cytoskeleton destruction, mathematical model.*

Arrived: 1 July 2020
Revision accepted: 25 September 2020
Correspondence: Elena Kozlova
e-mail: waterlake@mail.ru

INTRODUCTION

Long-term storage (up to 42 days) of packed red blood cells (PRBC) causes morphological, structural, and functional changes in the red blood cells (RBC)[1]. Clinicians separate

Blood Transfus 2021; 19: 124-34 DOI 10.2450/2020.0220-20
© SIMTIPRO Srl

All rights reserved - For personal use only
No other use without premission

© SIMTIPRO Srl

transfused PRBC into "fresh" and "old" products[2]. Post-transfusion complications have been shown to occur more frequently and in a more severe form in recipients of "old" RBC than in those given "fresh" RBC[2-4].

According to the duration of storage, biochemical and biophysical parameters of PRBC change[5-8]: pH decreases, lactate concentration increases, and extracellular K^+ concentration increases. There are also changes in the membranes of RBC: the stiffness of the membranes increases[3,9], membrane microvesicles form[10,11], the nanosurface of membranes alters[12,13], and reversible and irreversible morphological changes develop[12-14].

The main reason for impairments in RBC membrane structure during storage of PRBC ("storage lesions") is oxidative stress, which increases during the storage period[5,7]. The direct reason for the change of cellular morphology and decrease of the cells' elasticity during long-term storage of PRBC is due to structural changes of the cytoskeleton of the RBC[8,12].

The mechanism causing changes of cellular membranes has not been fully studied. Until the mechanism of structural modifications of cellular membranes is clear, it will be difficult to select optimal conditions for long-term storage of PRBC and thereby avoid irreversible changes[15]. Experimental methods that make it possible to register structural alterations of the cytoskeleton of RBC during storage would facilitate the study of the mechanism of membrane impairment. Atomic force microscopy has been found to be an effective method for studying the transformation of the organisation of the cytoskeletal mesh during PRBC storage and for obtaining a qualitative evaluation of its parameters[16-19]. Using this method, we evaluated the kinetics of structural transformations in the cytoskeleton of RBC under long-term storage (up to 42 days).

MATERIALS AND METHODS

Packed red blood cells

Six packs of RBC were obtained at blood transfusion clinical sites in Moscow, Russian Federation. The PRBC were stored in citrate-phosphate-dextrose (CPD) - saline, adenine, glucose, mannitol (SAGM)[7] solution at a temperature of +4 °C (in accordance with World Health Organization recommendations)[20]. Samples for in vitro experiments were taken from the bags on storage days 3, 12, 19, 21, 24, 28, 35, and 42.

Red blood cell ghosts

To obtain images of the cytoskeletal network and its individual constituents, RBC ghosts were formed. Components of the solution in which the RBC were stored were removed. In order to do this, we took 50 µL of PRBC mixed with 500 µL of phosphate-buffered saline (PBS) at pH 7.4 (MP Biomedicals LLC, Illkirch-Graffenstaden, France). This suspension was stirred on a mini-rotator Bio RS-24 (Biosan, Rīga, Latvia) with a rotation frequency of 6-8 rpm for 5 min. This step was important for a thorough, uniform, slow RBC washout from the storage solution. The suspension was then centrifuged at 1,500 rpm for 5 min in a centrifuge Universal 320 (Andreas Hettich GmbH & Co. KG, Tuttlingen, Germany). After removal of the supernatant fluid, 75 µL of sediment cells remained. Next, 500 µL of PBS were added. The washing process was repeated five times. The next stage was haemolysis of the RBC, which was achieved by adding 500 µL of hypotonic solution (0.09% NaCl in distilled water) to the cells. The suspension obtained was centrifuged at 3,000 rpm for 5 min. The supernatant was removed, and 300 µL of distilled water were added. Finally, the derived sample was placed in a refrigerator at 4°C for 30 min, after which the mixture was kept for 10 min at 20°C. The RBC ghosts formed in the resulting solution. The suspension obtained was centrifuged at 3,000 rpm for 5 min. The supernatant was removed and the 10 µL of sediment were used to prepare a ghost monolayer smear on a glass slide, using a V-Sampler® device (Vision, Vienna, Austria). The ghost monolayer was scanned with an atomic force microscope (AFM). No membrane fixatives, including glutaraldehyde, were used at any stage of the preparation of the cytoskeletal mesh. The procedure used to obtain the RBC ghosts has been described in detail previously[17].

Atomic force microscopy

The RBC ghosts were scanned with an AFM NTEGRA Prima (NT-MDT Spectrum Instruments, Moscow, Russian Federation) in the tapping mode. NSG01 cantilevers (TipsNano, Tallinn, Estonia) with the following characteristics were used: force constant 5 N/m, tip curvature radius 10 nm, resonant frequency 87-230 kHz. For image processing we used SPM Nova PX software (NT-MDT Spectrum Instruments). The number of scan points was 1,024×1,024 and the scanning

© SIMTIPRO SRL

All rights reserved - For personal use only
No other use without premission

fields were 100×100 μm², 10×10 μm², 2.5×2.5 μm², and 0.5×0.5 μm².

Young's modulus of elasticity for native RBC was studied using atomic force spectroscopy (AFS). A cantilever series SD-R150-T3L450B-10 (Nanosensors™, Neuchatel, Switzerland) was used (resonant frequency 21 kHz, stiffness coefficient 1 N/m). Force curves were measured on native RBC deposited on glass with polylysine (MP Biomedicals LLC, Illkirch-Graffenstaden, France) in an AFM open liquid cell, without using chemical fixatives. We mapped the force curves and used the Hertz model to calculate Young's modulus. Statistical processing was performed based on at least 100 force curves for each day of measurement. Details of the methods to prepare samples and calculate Young's modulus were described by Manchenko *et al.*[9].

Methods of blood analysis

The general analysis of PRBC was performed with an ADVIA 60 analyser (Bayer HealthCare LLC, Tarrytown, NY, USA). A Miura One blood analyser (I.S.E. S.r.l, Rome, Italy) was used to quantify lactate and glucose. An I-510 ionometer (NPO Akvilon, Podolsk, Russian Federation) was used to measure pH with an ES-10603 electrode and an ESR-10103 reference electrode and the concentration of extracellular potassium in PRBC using a potassium ion-selective electrode.

Statistical analysis

For each of the test days during storage, three smears of ghost monolayers were prepared from each bag of PRBC. For each of the three smears, five images sized 100×100 μm² were taken from various parts of the smear and five images sized 50×50 μm². To analyse the nanostructure of the cytoskeletal network, a 2.5×2.5 μm² section on 30 ghosts was scanned. Detailed analysis and spectral decomposition of the nanostructure of cytoskeletal fragments was performed on 0.5×0.5 μm² scans (20-30 fragments). A total of 280-300 images were obtained per pack. Overall, 1,710 images from six packs were analysed.

Using Image Analysis 3.5 software (NT-MDT Spectrum Instruments), parameters of cytoskeletal configuration were calculated: the area of a single pore, A, the perimeter of pores, P, the height of the cytoskeleton nanostructure, the number of pores, and the sum of their areas in a specified size of a sample.

Statistical analysis was performed using OriginPro 2019 software (OriginLab Corporation, Northampton, MA, USA) and included calculation of the mean, standard error, mode, skewness, histograms, calculation, and construction of theoretical and empirical functions of distribution, and non-linear fitting to find unknown approximation parameters. One-way analysis of variance was used and p-values <0.05 were considered statistically significant.

RESULTS

Cytoskeleton of packed red blood cells during long-term storage

Atomic force microscopy images of the red blood cell cytoskeleton

In the preparatory stage, RBC ghosts were formed (**Figure 1a**), and images of individual cytoskeletal fragments in the field of the AFM were obtained. **Figure 1b** shows a 1×1 μm² fragment of cytoskeleton in three-dimensional format, with its basic components.

The configuration of the network of the RBC cytoskeleton is determined by the structure of the spectrin matrix, which is the basis of the cytoskeleton. Structural impairment of the spectrin matrix causes changes in the organisation of the cytoskeletal mesh.

Figure 1 shows light areas (protein filaments of the cytoskeleton) and dark areas (cytoskeletal holes or pores). The bottom of the pores of the cytoskeleton is made up of lines with an underlayer (basal surface) (**Figure 1a**), on which the cytoskeleton lies[17]. The cytoskeleton has a pseudohexagonal configuration, which consists of cytoskeletal filaments and pores (**Figure 1b**). This figure shows examples of pores, fine (thin), clustered, and broken (ruptured) cytoskeletal filaments.

Figure 1c shows images of the cytoskeleton network images on storage days 3, 21, and 42. The thickness of the cytoskeletal network is the height of the pores above the basal surface, which is fixed in the experiment, and was 5-8 nm (colour scale of heights in **Figure 1c**), and is comparable to the thickness of the spectrin network[21,22].

Parameters of packed red blood cell cytoskeleton

The following parameters of the cytoskeletal network were calculated: area (A) and perimeter (P) of a single pore, number (N) of pores per fragment of a selected size, average area (A_{mean}) and perimeter (P_{mean}) and their corresponding deviations (σ_A and σ_P, respectively). The values of A (μm²) and P (μm) were statistically distributed

Blood Transfus 2021; 19: 124-34 DOI 10.2450/2020.0220-20

© SIMTIPRO Srl

All rights reserved - For personal use only
No other use without premission

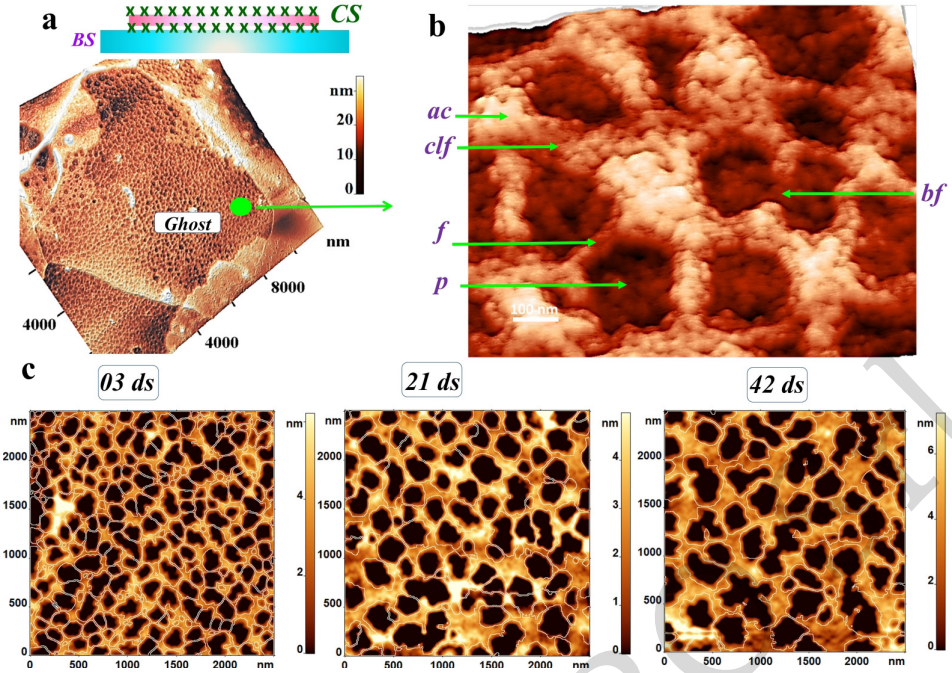


Figure 1 - Atomic force microscopy images of the red blood cell cytoskeleton
(a) Ghost formation and atomic force microscopy (AFM) image of a 12×12 µm² fragment (in phosphate-buffered saline), CS: cytoskeletal network, BS: basal surface; (b) CS fragment 1×1 µm² in three-dimensional format showing examples of pores (p) and of filaments labelled as fine (thin) (f), clustered (*clf*), and broken (*bf*). (c) Fragments of CS 2.5×2.5 µm² at days (ds) 3, 21, and 42 of storage of packed red blood cells in a flat two-dimensional format with pore segmentation. A colour scale of heights is given for all images. The AFM images of CS fragments were obtained in air.

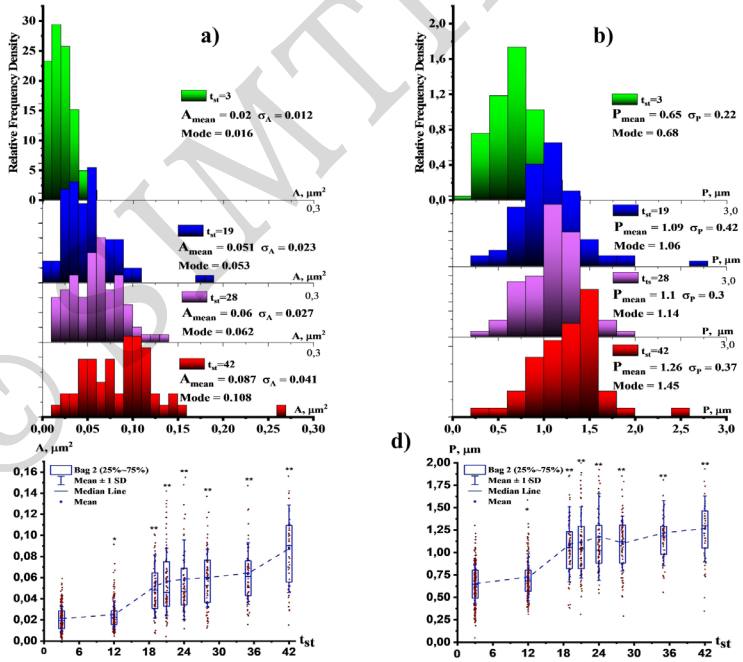


Figure 2 - Changes of the parameters of the cytoskeletal network at 3, 19, 28, and 42 days of storage for pack n. 2
(a) Histograms of relative frequency density for pore areas (A). (b) Histograms of the relative frequency of pore perimeters (P); (c, d) Graphs of increase of means of areas, A, and perimeters, P, of pores on storage days 3, 12, 19, 21, 24, 28, 35, and 42. Data in boxes represent the 25th to the 75th percentiles, whiskers show the mean standard deviation. The horizontal line indicates the median and the square indicates the mean. Dots show experimental data: The number of pores considered for the A and P measurements are shown in **Table I**. A dotted line connects the mean for each storage day. *p<0.05, **p<0.01 compared to storage day 3.

All rights reserved - For personal use only
No other use without premission

on any day of observation and corresponding histograms were therefore created to describe them (**Figure 2**). **Figure 2a,b** shows histograms of the density of relative frequencies for A and P of cytoskeletal pores for 3, 19, 28, and 42 days for pack n. 2.

The average value of the areas of single pores on day 3 was 0.020 μm^2, and the mean standard deviation was 0.012. By storage day 42, the average area had increased to 0.087 μm^2 (a 4.3-fold increase) and σ had increased from 0.012 to 0.041 (a 3.4-fold increase). Thus, as the storage duration increased, the cytoskeleton pores changed from being small to being larger. By day 42, there were two modes in the distribution of the area: 0.053 μm^2 and 0.108 μm^2, with this latter value being double the former. Thus, the most probable event was coalescence of two small pores to form a large one (although, seemingly, there were other combinations). Maximal parameter A mode increased from 0.016 μm^2 to 0.108 μm^2 (an increase of. 6.75-fold). The average pore perimeter almost doubled by day 42, from 0.65 to 1.26 μm), and σ increased 1.7-fold. By this time, the average value of Young's modulus (E) of PRBC membranes increased 2.3 times compared to E on day 3. Thus, by the end of the storage period, the stiffness of RBC membranes had increased significantly.

The average values of A and P increased in a non-linear fashion with PRBC storage (**Figure 2c,d**). Thus, prior to day 19, the average rate of increase in the areas of single pores was 3×10^{-4} μm^2/day, whereas from day 19 until day 42 the average rate of increase was 20×10^{-4} μm^2/day, i.e. an increase of 2.9-fold.

Similar tendencies were seen for the increase of average values of pore perimeters. The increase in size of separate pores led to a decrease in the number of pores in a selected area, due to the merging of small pores into larger ones with rupture of the filaments of the cytoskeleton.

The sum of areas, ΣA (μm^2), of all the pores in same-sized fragments (2.5×2.5 μm^2) barely changed. Over the whole period of storage of PRBC, ΣA only changed 1.2-fold (**Table I**); the number of pores decreased by 5.1-fold during the same period. In the first 24 days, the ΣA ranged from 74-83% of the fragment area, i.e. it almost did not change (despite the number of pores decreasing by 2.6-fold during the period). In other words, there was a redistribution of the sizes of separate pores and their numbers in selected fragment areas during the entire time of PRBC storage: the area of individual pores increased, but the number of pores in a selected fragment area decreased. The numerical values of these

Table I - *Average values of the area (A) and perimeter (P) of pores in membranes of red blood cells in each of six packs (1-6) on storage days 3, 19, 28, and 42*

	3 day	19 day	28 day	42 day
Pack 1				
P (μm)	0.73 (0.25)	0.82* (0.35)	1.08** (0.45)	1.09** (0.45)
A (μm^2)	0.025 (0.015)	0.032 (0.018)	0.049** (0.018)	0.050** (0.022)
Pack 2				
P (μm)	0.65 (0.22)	1.09** (0.42)	1.10** (0.30)	1.26** (0.37)
A (μm^2)	0.020 (0.012)	0.051** (0.023)	0.060** (0.027)	0.087** (0.041)
Pack 3				
P (μm)	0.69 (0.20)	0.83* (0.25)	0.95** (0.35)	1.18** (0.45)
A (μm^2)	0.026 (0.014)	0.034 (0.027)	0.047** (0.027)	0.056** (0.035)
Pack 4				
P (μm)	0.66 (0.25)	0.77* (0.27)	0.95** (0.33)	1.22** (0.40)
A (μm^2)	0.022 (0.015)	0.034 (0.027)	0.038** (0.027)	0.062** (0.028)
Pack 5				
P (μm)	0.73 (0.22)	0.83* (0.35)	0.99** (0.40)	1.43** (0.50)
A (μm^2)	0.026 (0.014)	0.032 (0.027)	0.043** (0.029)	0.078** (0.035)
Pack 6				
P (μm)	0.65 (0.19)	0.68 (0.25)	0.95** (0.30)	1.80** (0.50)
A (μm^2)	0.022 (0.012)	0.023 (0.018)	0.043** (0.025)	0.125** (0.045)
Sum of pore areas: ΣA μm^2	4.8±0.4 (77%)	4.9±0.4 (78%)	4.6±0.3 (74%)	4.2±0.3 (67%)
Number of pores, N	242±26	96±18**	76±12**	47±4**

The sum of pore areas (ΣA, μm^2), the ΣA as a percentage of the fragment area (% ΣA) and the number of pores, N, in the fragments (2.5×2.5 μm^2) (pack n. 2) are shown. Data are reported as mean (standard deviation). *p<0.05, **p<0.01 compared to day 3 of storage.

Blood Transfus 2021; 19: 124-34 DOI 10.2450/2020.0220-20

© SIMTPRO.SI
All rights reserved - For personal use only
No other use without premission

parameters for pack n. 2 for the days of the experiment are given in **Table I**. Similar tendencies were observed for all the study packs.

Three states of cytoskeleton filaments

AFM images of the cytoskeletal network after storage of PRBC for various periods (**Figure 1c**, **Figure 2a-c**) show that cytoskeletal filaments can be viewed as a statistical ensemble of elements. Each element can exist in one of three states: as a single fine filament (*f*), as a ruptured broken filament (*bf*) and as a thickened clustered filament (*clf*).

- **State *f*** (**Figure 3a-c**). The initial size of separate nanostructures of the filament, particularly its grain (**Figure 3b**), was a_f=37±5 nm, (profile section 2-2). Profile section 1-1 has three fixed grain structures, located along the filament. A three-dimensional image (**Figure 3c**) has a separate grain shown in a circle. Sections 1-1 and 2-2 correspond to lines of profile measurements, yellow arrows correspond to the vertical dotted lines on the respective profiles. For all images, colour scales of heights are shown. We used the method of spatial Fourier transformation for AFM image deconvolution, as described in our previous study[23]. The structure size was estimated at the 0.7 level.
- **State *clf*** (**Figure 3d-f**). Cytoskeleton filament thickness is increased. **Figure 3e** shows an example of a thickened filament structure with a characteristic size a_{clf}=120±10 nm (122 nm in the 2-2 profile), which is approximately three times greater than that of *f* filaments. The filament cytoskeleton on day 3 consisted of one row of protein grains located along line 1-1 (**Figure 3b,c**). On storage day 42, the filament cytoskeleton consisted of several rows of protein granules also located alongside, but the entire structure was a complicated granular conglomerate (**Figure 3e,f**). The size of a single granule remained, in this case, practically unchanged at 37±5 nm (shown in a circle in **Figure 3f**).
- **State *bf*** (**Figure 4a,b**). As a result of the effect of physical and chemical agents on blood, cytoskeleton filaments may rupture. **Figure 4** shows examples of AFM images of typical ruptures, which develop during the storage

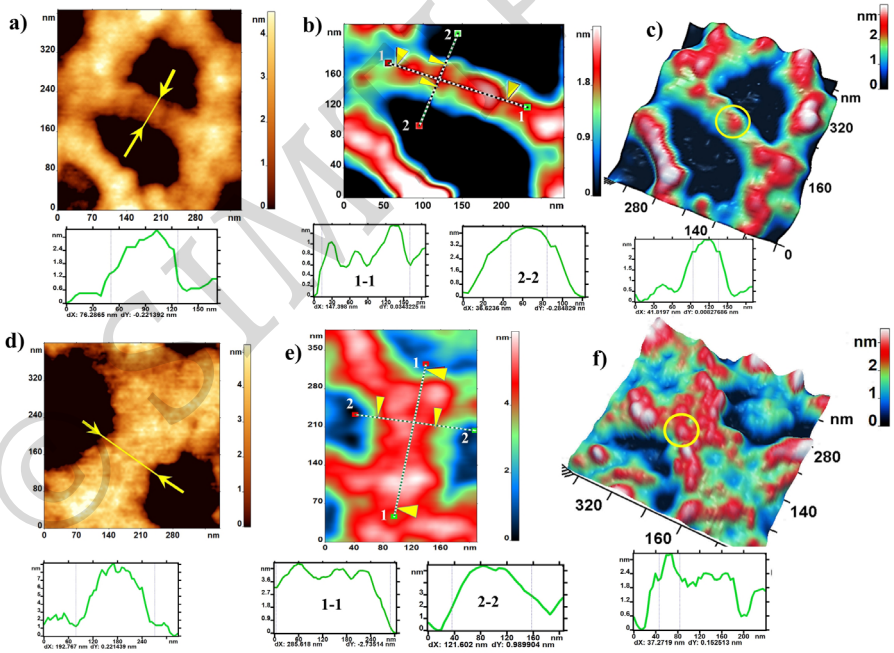


Figure 3 - States of cytoskeletal filaments
(a-c) Thin single filament (in state *f*) on storage day 3. (a) Initial atomic force microscopy (AFM) image of the filament (shown by arrows) and its profile. (b) Two-dimensional AFM image of this filament: second order of the spatial Fourier transformation: 1-1 and 2-2 correspond to lines of profile measurements, yellow arrows correspond to the vertical dotted lines on the respective profiles. (c) Three-dimensional image and profile of a separate grain shown in a yellow circle. (d-f) Clustered thickened filament (in state *clf*) on storage day 42. (d) Initial AFM image of the clustered filament (shown by arrows) and its profile. (e) Two-dimensional AFM image of this filament: second order of the spatial Fourier transformation, 1-1 and 2-2 correspond to lines of profile measurements, yellow arrows correspond to the vertical dotted lines on the respective profiles. (f) Three-dimensional image and profile of a separate grain shown in a yellow circle. A colour scale of heights is given for all graphs. The method of spatial Fourier transformation for AFM image deconvolution was described in our previous study[23]. AFM images of cytoskeletal fragments were obtained in air.

All rights reserved - For personal use only
No other use without premission

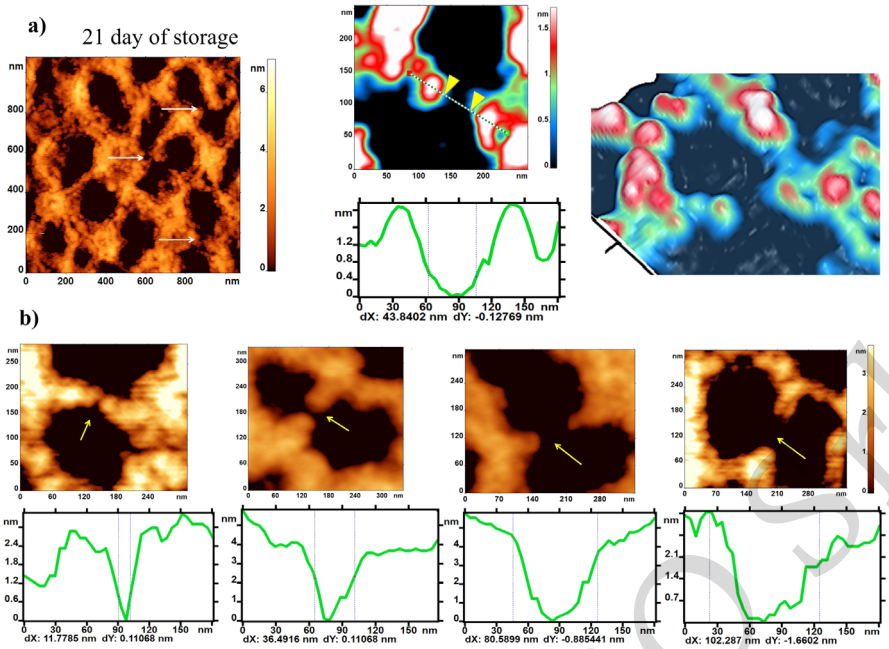


Figure 4 - The process of destruction (rupture) of cytoskeletal filaments (*bf* state) at day 21 of storage of packed red blood cells
(a) Left: atomic force microscopy (AFM) image of a 1×1 μm² fragment of the cytoskeletal network, the arrows point to examples of broken filaments; centre: an image of a breaking filament (the second order of spatial Fourier transformation) and its profile; right: three-dimensional image of fragment rupture. (b) Filament rupture (shown with arrows). From left to right, the beginning of the rupture and subsequent stages of the rupture with the corresponding profiles of the broken filaments underneath; profile lines are selected in the same way as in image (a). Colour scales of height are shown for the images. The method and orders of spatial Fourier transformation are described elsewhere[23]. AFM images of cytoskeleton fragments were obtained in air.

of PRBC intended for transfusion. We observed rupture sizes a_{bf} from 10 to 200 nm (complete filament destruction). Thus, **Figure 4b** shows a continuous increase of rupture: 12-36-80-102 nm. Broken filaments were seen in the RBC matrix under physiological conditions as well. This is why the average value of the pore sizes in control samples were statistically distributed (**Figure 2a, b**).

As a result of filament rupture during storage, the cytoskeleton pores merge, their area increases by 2- to 3- fold, and the nanostructure and morphology of the cells change.

Kinetic model of the rearrangement of structural organisation of the cytoskeleton

Cytoskeleton as a statistical ensemble of the elements

The cytoskeletal network (**Figures 1** and **5a,b**) is seen as a statistical ensemble of elements in three states *f, b, clf*. A schematic presentation of the filaments and cytoskeleton network is shown in **Figure 5c-e**. The number of elements in a specific state changes dynamically with the duration of storage of PRBC.

Figure 5f shows the correlation between the amount (N_f) of normal matrix filaments and the time of storage, t_{st}: N_f/N_{f0} (t_{st}). Standardisation was performed considering the average value of the number of normal filaments at the beginning of storage (t_{st}=0).

Kinetic equation to measure the number of filaments in various conditions

Given N_f (t_{st}), i.e. the dependence of the number of undamaged cytoskeletal thin filaments on the storage time of PRBC (in a single area), the kinetic equation of the measurement $N_f(t_{st})$ can be described:

$$\frac{dN_f}{dt_{st}} = -\left(\frac{dN_f}{dt_{st}}\right)_{bf} - \left(\frac{dN_f}{dt_{st}}\right)_{clf} \qquad [1]$$

initial condition N_f (t_{st}=0)=N_{f0}, where: $\frac{dN_f}{dt_{st}}$ is the rate of change of the number of filaments in condition *f*, $-\left(\frac{dN_f}{dt_{st}}\right)_{bf}$ is the rate of decrease of filaments due to their rupture, and $-\left(\frac{dN_f}{dt_{st}}\right)_{clf}$ is the rate of decrease of filaments due to the process of thickening as a result of cluster formation and protein aggregation.

The initial cause of filament rupture and cluster formation is an alteration of molecular processes in the cells, mainly

Blood Transfus 2021; 19: 124-34 DOI 10.2450/2020.0220-20

All rights reserved - For personal use only
No other use without premission

© SIMTIPRESS

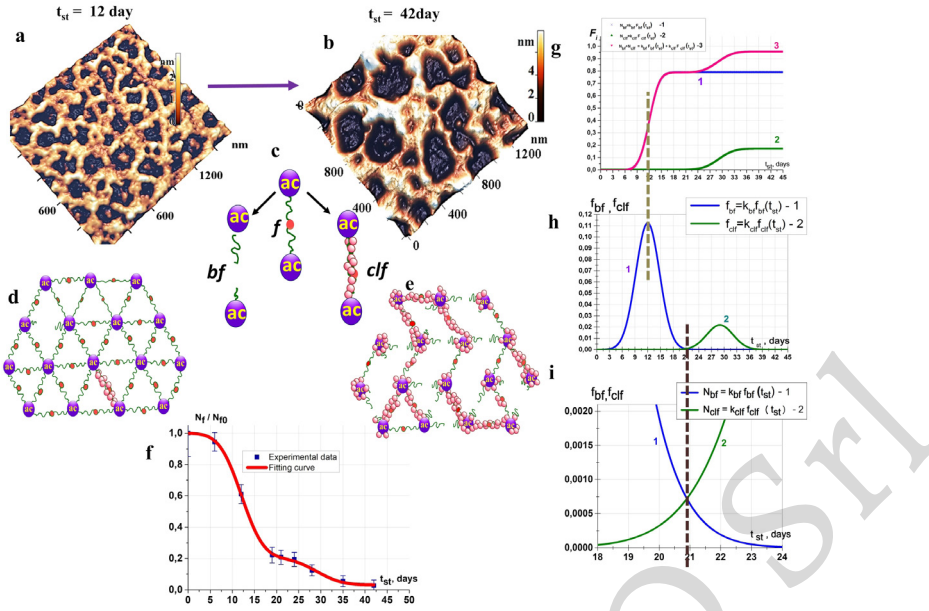


Figure 5 - Change in the state of cytoskeleton filaments and a two-stage process of cytoskeletal damage during storage of packed red blood cells. Cytoskeletal network

(a) Three-dimensional atomic force microscopy (AFM) image of a 1.8×1.8 μm² fragment of the cytoskeleton of packed red blood cells on storage day 12. (b) The same type of image on storage day 42. AFM images of cytoskeletal fragments in (a, b) were obtained in air. (c) Schematic image of a single, thin filament (*f*), a broken filament (*bf*), a clustered filament (*clf*), and actin complex (ac). (d, e) Scheme of cytoskeletal fragments in a control sample (t_{st}=3 days) (d) and after prolonged storage (t_{st}=42 days) (e). (f) Kinetics of the change in the number of thin filaments, experimental data (blue squares), and fitted curve (continuous red line) (Eq[3]) considering detected parameters of the model k_{bf}=0.79, μ_{bf}=12 days, σ_{bf}=2.8 days, k_{clf}=0.17, μ_{clf}=29 days, μ_{clf}=3.1 days for pack n. 2. (g) Theoretical kinetic curves of filaments appearing in state *bf* (blue line), in state *clf* (green line) and their total (red line). (h) Rate of development of cytoskeletal filaments in conditions *bf* and *clf*; (i) Curves on a larger scale, with the moment of alignment of the rates. Function parameters correlate to those in (f). Data from pack n. 2

as a result of an increase in the concentration of reactive oxygen species (ROS)[7]. Filaments have various thresholds of ruptures $t_{st\ thr\ bf\ i}$, which are an inherent characteristic for each given filament *i*. In order for a filament *i* to rupture, it must be affected by specific concentrations of pathogenic factors. The concentrations of such factors increase the longer the storage time $t_{st\ i}$. Let us suppose that the storage time required for breaking a filament has a Gaussian distribution (normal distribution law):

$$f_{bf}(t_{st}) = \frac{1}{\sqrt{2\pi}\sigma_{bf}} e^{-\frac{(t_{st}-\mu_{bf})^2}{2\sigma_{bf}^2}} \quad [2]$$

where: μ_{bf} is the average value of $t_{(st\ thr\ bf)}$, and σ_{bf} is the mean square deviation. At a given time of storage, t_{st} of PRBC, only those filaments *i* that have a rupture threshold $t_{(st\ thr\ bf\ i)}<t_{st}$ are going to break. A similar pattern holds for processes of protein cluster formation and, accordingly, filament thickening.

Average values and mean square deviations for the distributions of *bf* and *clf* generally vary.

The solution of equation [1] is therefore:

$$N_f(t_{st})/N_0 = 1 - k_{bf}F_{bf}(t_{st}) - k_{clf}F_{clf}(t_{st}) \quad [3]$$

where:

$$F_{bf}(t_{st}) = \int_{-\infty}^{t_{st}} \frac{1}{\sqrt{2\pi}\sigma_{bf}} e^{-\frac{(t_{st}-\mu_{bf})^2}{2\sigma_{bf}^2}} dt_{st},\ F_{clf}(t_{st}) = \int_{-\infty}^{t_{st}} \frac{1}{\sqrt{2\pi}\sigma_{clf}} e^{-\frac{(t_{st}-\mu_{clf})^2}{2\sigma_{clf}^2}} dt_{st} \quad [4]$$

Coefficients k_{bf} and k_{clf} show the percentages of initial filaments participating in the rupture process and cluster formation.

Non-linear curve fitting of experimental data $N_f\ (t_{st})_{exp}/N_0$ (**Figure 5f**) was performed using OriginPro 2019 software. For this, a theoretical function was used (Eq[3]). Model parameters k_{bf}, μ_{bf}, σ_{bf}, k_{clf}, μ_{clf}, σ_{clf}, were unknown. These model parameters were chosen such that the theoretical curve best described the experimental data with an approximate R^2>0.98.

Figure 5f (red curve) shows the theoretical approximation function (Eq[3]) of the relation between the number

All rights reserved - For personal use only
No other use without premission

© SIMTIPRO Srl

of filaments in state *f* and the PRBC storage time, depending on the existing unknown parameters: k_{bf}=0.79, μ_{bf}=12 days, σ_{bf}=2.8 days; k_{clf}=0.17, μ_{clf}=29 days, σ_{clf}=3.1 days.

Two stages of reconfiguration of the cytoskeletal network

This study utilizes a model which shows good correlation between the kinetics of the decrease in the number of cytoskeleton filaments in the experiment and the obtained kinetic curve of approximation (**Figure 5f**). This confirms the adequacy of the mathematical model presented. When describing the impairment of initial normal cytoskeletal filaments (*f*), it is adequate to consider the superposition of two processes - filament rupture (*bf*) and clustering of the filaments (*clf*).

As a result of approximation, the parameters obtained allowed us to calculate separately the time dependencies of elements in the *bf* (**Figure 5g**, **blue line**) and *clf* (**Figure 5g**, **green line**) states. The red line in **Figure 5g** shows the overall dependence $\frac{N_{bf}(t_{st})}{N_0} + \frac{N_{clf}(t_{st})}{N_0}$ which makes it possible to calculate the total number of cytoskeletal filaments *f* damaged due to rupture and cluster formation. The rates of rupture and cluster formation of the filaments are show in **Figure 5h, i**.

A true statistical difference of the μ_{bfmean} and $\mu_{clfmean}$ ($p<0.01$) confirms that there is a two-stage process of damage of cytoskeleton configuration during the long-term storage of PRBC. This correlates well with the findings of other authors that different types of lesions develop at their own specific times[7,8,24].

First, the process of filament rupture starts. The rupture of *f* starts actively by days 9-10. By the end of week 2 of storage, μ_{bf}=13±1 days, and the rate of this process reaches its maximum. By days 18-21, proteins begin to cluster and the cytoskeletal filaments thicken; the rate of filament thickening reaches a maximum by μ_{clf}=30±3 days. The percentages of filaments that rupture and form clusters are significantly different. On average, k_{bf}=0.70±0.09 and k_{clf}=0.19±0.02, which means that 10% of filaments remain in the original condition *f*.

Parameters of the packed red blood cell storage solution

During storage of the PRBC, pH, glucose concentration, extracellular K^+ concentration, lactate level, and general blood biochemical parameters were recorded. The mean pH value of the six packs on RBC on day 3 was 7.2±0.2. By the end of storage on day 42, the mean pH value was 6.3±0.4. Between days 19 and 23, pH values were 7.0-6.8. Extracellular K^+ concentration increased from 3.4±0.1 mmol/L (on day 3) to 18±3 mmol/L (on day 42). Glucose concentration dropped from 20±2.3 mmol/L (on day 3) to 14±2.5 mmol/L (on day 42), while the lactate concentration increased from 5.5±2.1 mmol/L (on day 3) to 21±3 mmol/L (on day 42). These results are consistent with those obtained previously[12].

DISCUSSION

Two stages of impairment of the structural organisation of the cytoskeleton

When storing PRBC for 42 days, the main alterations in the cytoskeletal network are rupture of cytoskeletal filaments (**Figures 1b**, and **4**), merging of small pores into larger ones, and thickening of the filaments (**Figure 3d-f**). These effects develop in a non-linear manner. In the middle of the storage period, after the end of the first stage, the filaments break and the second process begins with protein cluster formation (**Figure 5g-i**). Irreversible cluster formation in the cytoskeleton begins on days 19-21. This correlates with the time when the rate of large pore formation increases, the overall number of pores decreases, and the rigidity of RBC membranes increases. It is at this time when the possibility of post-transfusion complications increases[1,2].

What is the molecular mechanism underlying each stage? As PRBC are stored longer, the concentration of ROS increases[7]. An analysis showed a strong correlation (r=0.99) between the increase of ROS concentration[7] and the increase in the number of broken cytoskeletal filaments in our experiments (**Figure 5g**, **curve 1**). As a result, the spectrin-ankyrin-band 3 bond is broken, filaments rupture, and a large proportion of spectrin tetramers are dissociated into dimers[25]. In unperturbed cells, a small percentage of the tetramer population is dissociated into dimers, but the effect of external factors results in the proportion of spectrin dissociated into dimers increasing to 70-75%[25,26], which agrees with the submitted experimental data (**Figure 5g**).

Oxidative stress in membranes, which causes oxidation and aggregation of proteins, may, in the end, lead to thickening of cytoskeletal elements. The following processes occur: obstacle-free diffusion of transmembrane

© SIMTIPRO Srl

All rights reserved - For personal use only
No other use without premission

proteins with dissociation of spectrin tetramers and their clustering; band 3 oligomerisation and/or aggregation[27]; binding of high-molecular-weight aggregates of proteins with the membrane[28]; accumulation of oxidised proteins at the cytoskeleton elements[25,29,30]; haemoglobin degradation and stronger binding of degraded haemoglobin to the membrane[28]; and denaturation of hemichromes into haemin, globin, and free molecular iron[31].

One of the most harmful, irreversible, oxidative protein modifications is carbonylation[32,33]. It was previously found that carbonylation in the cytoskeletal membrane fraction increases significantly after the third week of storage in CPD-SAGM and, in particular, between days 29 and 42 of storage[33]. With the increased concentration of protein carbonyls, the possibility of protein aggregation increases, with association of proteins in large ensembles[34]. The aggregation process can be viewed as a first order phase transition that starts with a critical concentration of oxidized proteins[35], which is achieved by day 30 of PRBC storage[7]. Our results correlate with these findings.

Consequences of cytoskeleton configuration impairment

By days 9-16 of storage topological nanodefects develop in membranes, confirming the rupture of cytoskeleton filaments[12]. Such topological defects have been observed following exposure of blood to the oxidizing agent hemin[23], during gamma-radiation of cells prior to transfusion[36], when red blood cells have been stored without special solutions[13], and with coral proteins affecting the blood[37].

The negative effect of protein cluster formation and thickening of cytoskeletal filaments is an increase of the stiffness of RBC membranes. By day 21, band 3 in the membrane starts to cluster[27], and membrane rigidity increases significantly by week 4 (28 days)[3]. It has been suggested that protein aggregation into insoluble deposits protects from oxidative stress[38]. The described rearrangements of the cytoskeleton are a major cause of functional disorders of stored RBC. These phenomena can reduce the effectiveness of blood transfusions and increase the risk of post-transfusion complications when PRBC have been stored for more than 19-24 days.

CONCLUSIONS

This study utilising AFM and atomic force spectroscopy shows in an experimental setting that, with long-term storage of PRBC (42 days), the main events in the cytoskeletal network are rupture of filaments, merging of small pores into larger ones, a decrease in the number of pores, thickening of filaments, and increase of membrane stiffness. These effects develop in a non-linear manner, with irreversible processes in the RBC cytoskeleton starting at days 19-21.

Experimental studies and a kinetic model showed two stages of the process of damage to the cytoskeletal elements and showed the typical timing and specifics of these stages.

Destruction of the molecular organisation of the cytoskeletal network of RBC leads to altered morphology and deformity of cells in the blood circulation. These changes can have a negative effect on the efficacy of blood transfusions and increase the risk of post-transfusion complications. The results of this study can be used in clinical medicine to evaluate the quality of PRBC intended for transfusion, during the analysis of post-transfusion complications that develop when transfusing PRBC stored for different periods, and when performing biophysical studies of the molecular organisation of RBC under various physical and chemical conditions.

ACKNOWLEDGEMENTS

This work was supported by the Ministry of Science and Higher Education of the Russian Federation and by the "Russian Academic Excellence Project 5-100".

AUTHORS' CONTRIBUTIONS

AC and EK suggested the idea of studying the structure of cytoskeleton of packed red blood cells during long-term storage and designed the atomic force microscopy experiments. VS, ES and OG conducted the experiments. VS and ES performed atomic force microscopy scanning, processed images and prepared figures. AK, AC and EK suggested mechanisms and created the mathematical models. VM and AC discussed the results and interpreted data. EK and AC wrote the main manuscript text together with VM. All Authors reviewed the manuscript.

The Authors declare no conflicts of interest.

All rights reserved - For personal use only
No other use without premission

© SIMTIPRO Srl

REFERENCES

1. Yoshida T, Prudent M, D'Alessandro A. Red blood cell storage lesion: causes and potential clinical consequences. Blood Transfus 2019; **17**: 27-52.
2. García-Roa M, Del Carmen Vicente-Ayuso M, Bobes AM, et al. Red blood cell storage time and transfusion: current practice, concerns and future perspectives. Blood Transfus 2017; **15**: 222-31.
3. Xu Z, Zheng Y, Wang X, et al. Stiffness increase of red blood cells during storage. Microsyst Nanoeng 2018; **4**: 17103.
4. Weinberg JA, McGwin G Jr, Vandromme MJ, et al. Duration of red cell storage influences mortality after trauma. J Trauma 2010; **69**: 1427-32.
5. D'Alessandro A, Yoshida T, Nestheide S, et al. Hypoxic storage of red blood cells improves metabolism and post-transfusion recovery. Transfusion 2020; **60**: 786-98.
6. Opoku-Okrah C, Acquah BK, Dogbe EE. Changes in potassium and sodium concentrations in stored blood. Pan Afr Med J 2015; **20**: 236.
7. D'Alessandro A, D'Amici GM, Vaglio S, Zolla L. Time-course investigation of SAGM-stored leukocyte-filtered red bood cell concentrates: from metabolism to proteomics. Haematologica 2012; **97**: 107-15.
8. Barshtein G, Arbell D, Livshits L, Gural A. Is it possible to reverse the storage-induced lesion of red blood cells? Front Physiol 2018; **9**: 914.
9. Manchenko E, Kozlova E, Sergunova V, Chernysh A. Homogeneous deformation of native erythrocytes during long-term storage. General Reanimatology 2019; **15**: 4-10.
10. Hess JR. Red cell changes during storage. Transfus Apher Sci 2010; **43**: 51-9.
11. D'Alessandro A. An update on red blood cell storage lesions, as gleaned through biochemistry and omics technologies. Transfusion 2015; **55**: 205-19.
12. Kozlova E, Chernysh A, Moroz V, et al. Morphology, membrane nanostructure and stiffness for quality assessment of packed red blood cells. Sci Rep 2017; **7**: 7846.
13. Girasole M, Dinarelli S, Boumis G. Structural, morphological and nanomechanical characterisation of intermediate states in the ageing of erythrocytes. J Mol Recognit 2012; **25**: 285-91.
14. Deryugina AV, Boyarinov GA, Simutis IS, et al. Morphological and metabolic parameters of red blood cells after their treatment with ozone. General Reanimatology 2018; **14**: 40-9.
15. Karon BS, Hoyer JD, Stubbs JR, Thomas DD. Changes in band 3 oligomeric state precede cell membrane phospholipid loss during blood bank storage of red blood cells. Transfusion 2009; **49**: 1435-42.
16. Swihart AH, Mikrut JM, Ketterson JB, Macdonald RC. Atomic force microscopy of the erythrocyte membrane skeleton. J Microsc 2001; **204** (Pt 3): 212-25.
17. Kozlova E, Chernysh A, Sergunova V, et al. Conformational distortions of the red blood cell spectrin matrix nanostructure in response to temperature changes in vitro. Scanning 2019; **2019**: 8218912.
18. Kozlova E, Chernysh A, Sergunova V, et al. Atomic force microscopy study of red blood cell membrane nanostructure during oxidation-reduction processes. J Mol Recognit 2018; **31**: e2724.
19. Liu F, Burgess J, Mizukami, Ostafin A. Sample preparation and imaging of erythrocyte cytoskeleton with the atomic force microscopy. Cell Biochem Biophys 2003; **38**: 251-70.
20. World Health Organization. Department of Blood Safety and Clinical Technology, Safe blood and blood product. *Manual on the management, maintenance and use of blood cold chain equipment*. Geneva: World Health Organization. 2005.
21. Li J, Lykotrafitis G, Dao M, Suresh S. Cytoskeletal dynamics of human erythrocyte. Proc Natl Acad Sci U S A. 2007; **104**: 4937-42.
22. Li H, Lykotrafitis G. Erythrocyte membrane model with explicit description of the lipid bilayer and the spectrin network. Biophys J 2014; **107**: 642-53.
23. Kozlova EK, Chernysh AM, Moroz VV, Kuzovlev AN. Analysis of nanostructure of red blood cells membranes by space Fourier transform of AFM images. Micron 2013; **44**: 218-27.
24. Prudent M., Tissot JD, Lion N . In vitro assays and clinical trials in red blood cell aging: lost in translation. Transfus Apher Sci 2015; **52**: 270-76.
25. Blanc L, Salomao M, Guo X, et al. Erythrocyte membrane-skeletal cohesion and its control of spectrin self-association. Biochemistry 2010; **49**: 4516-23.
26. An X, Lecomte M, Chasis JA, et al. Shear-response of the spectrin dimer tetramer equilibrium in the red blood cell membrane. J Biol Chem 2002; **277**: 31796-800.
27. Bosman GJ, Stappers M, Novotný VM. Changes in band 3 structure as determinants of erythrocyte integrity during storage and survival after transfusion. Blood Transfus 2010; **8**: s48-52.
28. Akoev VR, Matveev AV, Belyaeva TV, Kim YA. The effect of oxidative stress on structural transitions of human erythrocyte ghost membranes. Biochim Biophys Acta 1998; **1371**: 284-94.
29. Delobel J, Prudent M, Tissot JD, Lion N. Proteomics of the red blood cell carbonylome during blood banking of erythrocyte concentrates. Proteomics Clin Appl 2016; **10**: 257-66.
30. Kriebardis AG, Antonelou MH, Stamoulis K, et al. Progressive oxidation of cytoskeletal proteins and accumulation of denatured hemoglobin in stored red cells. J Cell Mol Med 2007; **11**: 148-55.
31. Yoshida T, Shevkoplyas SS. Anaerobic storage of red blood cells. Blood Transfusion 2010; **8**: 220-36.
32. Fedorova M, Bollineni RC, Hoffmann R. Protein carbonylation as a major hallmark of oxidative damage: update of analytical strategies. Mass Spectrom Rev 2014; **33**: 79-97.
33. D'Alessandro A, Zolla L. Biochemistry of red cell aging in vivo and storage lesions. Hematology Education: the education program for the annual congress of the European Hematology Association 2013; **7**: 389-96
34. Tanase M, Urbanska AM, Zolla V, et al. Role of carbonyl modifications on aging-associated protein aggregation. Sci Rep 2016; **6**: 19311.
35. Narayanan A, Meriin A, Andrews JO, et al. A first order phase transition mechanism underlies protein aggregation in mammalian cells. Elife 2019; **8**: e39695.
36. Al-Zahrani K, Al-Sewaidan H. Nanostructural changes in the cell membrane of gamma-irradiated red blood cells. Indian J Hematol Blood Transfus 2017; **33**: 109-15.
37. Díaz-Marrero AR, Rodríguez González MC, Hernández Creus A, et al. Damages at the nanoscale on red blood cells promoted by fire corals. Sci Rep 2019; **9**: 14298.
38. Carija A, Navarro S,de Groot NS,Ventura S. Protein aggregation into insoluble deposits protects from oxidative stress. Redox Biol 2017; **12**: 699-711.

© SIMTIPRO Srl

All rights reserved - For personal use only
No other use without premission